Dynamic Nuclear Polarization Enhanced Multiple Quantum Spin Counting of Molecular Assemblies in Vitrified Solutions

Mesopotamia S. Nowotarski,[*,†] Lokeswara Rao Potnuru,[*,‡] Joshua S. Straub,[¶] Raj Chaklashiya,[§] Toshihiko Shimasaki,[¶] Bholanath Pahari,[‖] Hunter Coffaro,[¶] Sheetal Jain,[⊥] and Songi Han[*,†,#,@]

†*Department of Chemistry and Biochemistry, University of California, Santa Barbara, Santa Barbara, California 93106 United States*

‡*Department of Chemistry, Northwestern University, Evanston 60208 Illinois, United States*

¶*Department of Physics, University of California, Santa Barbara, Santa Barbara, California 93106 United States*

§*Department of Materials, University of California, Santa Barbara, Santa Barbara, California 93106 United States*

‖*School of Physical and Applied Sciences, Goa University, Taleigao Plateau, Goa, 403206, India*

⊥*Solid State and Structural Chemistry Unit, Indian Institute of Science, Bangalore, 560012, India*

#*Department of Chemical Engineering, University of California, Santa Barbara, Santa Barbara, California 93106 United States*

@*Department of Chemistry, Northwestern University, Evanston 60208, Illinois, United States*

E-mail: mnowotarski@ucsb.edu; lokeswararao.potnuru@northwestern.edu; songi.han@northwestern.edu

Abstract

Crystallization pathways are essential to various industrial, geological, and biological processes. In nonclassical nucleation theory, prenucleation clusters (PNCs) form, aggregate and crystallize to produce higher order assemblies. Microscopy and X-Ray techniques have limited utility for PNC analysis due to small size (0.5 - 3 nm) and time stability constraints. We present a new approach for analyzing PNC formation based on ^{31}P NMR spin counting of vitrified molecular assemblies. The use of glassing agents ensures that vitrification generates amorphous aqueous samples, and offers conditions to perform dynamic nuclear polarization (DNP) amplified NMR spectroscopy. We demonstrate that molecular adenosine triphosphate, along with crystalline, amorphous, and clustered calcium phosphate materials formed via a non-classical growth pathway can be differentiated from one another by the number of dipolar coupled ^{31}P spins. We also present an innovative approach to examine spin counting data, demonstrating that a knowledge based fitting of integer multiples of cosine wave functions, instead of the traditional Fourier transform, provides a more physically meaningful retrieval of the existing frequencies. This is the first report of multi-quantum spin counting of assemblies formed in solution as captured under vitrified DNP conditions, which can be useful for future analysis of PNCs and other aqueous molecular clusters.

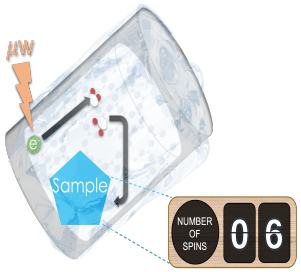

TOC Graphic.

Abbreviations	
Prenucleation Cluster	PNC
Dynamic Nuclear Polarization	DNP
Solid-State Nuclear Magnetic Resonance	ssNMR
Magic Angle Spinning	MAS
Rapid Freeze Quench	RFQ
Multiple Quantum Spin Counting	MQ-SC
Multiple Quantum Coherence	MQCO
Multiple / Double / Triple Quantum	MQ / DQ / TQ
Chemical Shift Anisotropy	CSA
Adenosine Triphosphate	ATP
Amorphous Calcium Phosphate	ACP
Hydroxyapatite	HAp
Modified Simulated Body Fluid	mSBF

Classical nucleation theory (CNT), where a nucleus of critical size grows by the addition of the elemental species (atoms, ions or molecules), does not fully explain crystalization pathways that utilize amorphous or mesocrystalline intermediates. Nonclassical nucleation theory encompasses all known deviations from CNT such as the synthesis of proteins, the formation of calcium carbonates, the growth of mesocrystals, etc.[1], wherein prenucleation clusters form from a supersaturated solution, and subsequently aggregate into a potential glassy intermediate, which then transforms into a crystalline phase. The recruitment of prenucleation clusters (PNCs) is essential to many nonclassical nucleation pathways. For example, the nucleation pathway of calcium phosphate is not well understood and proposed to be nonclassical[2,3]. Nonclassical growth pathways have significant potential for the development of materials with tunable functional complexity, such as modulating the density of intermediate states, due to additional states and more complex phase boundaries. To design such materials by nonclassical growth pathways, knowledge of the formation mechanism of PNCs is critical. However, PNCs remain mostly elusive to control due in significant part to the intrinsic difficulty of characterizing the highly dynamic structural evolution of prenucleation clusters. Microscopic and X-Ray techniques have been shown to offer some insight into the structure and dynamics of PNCs[4]; however, due to PNCs time transient nature in solution, these techniques are not sufficient or applicable for the study of most PNCs.

Low temperature solid-state nuclear magnetic resonance (ssNMR) is uniquely suited to offer atomic-scale structural information of PNC samples prepared at various time points in nonclassical growth pathways by vitrification at 100 K[5–8]. Vitrification by rapid cryogenic temperature transfer solidifies the sample into a glass rather than a crystalline structure by limiting the time atoms can rearrange into a crystalline orientation or an alternate temperature-dependent energetically favorable orientation, thus enabling the use of ssNMR on a sample that closely resembles the native state conditions. Sample vitrification without rapid freezing technology requires the use of a glassing agent. Plunge freezing of a solution containing 60 volume % glycerol into liquid nitrogen is currently the most widely used vitrification method for DNP experiments because at this condition, the glass quality of the sample is impervious to the cooling rate history and variation from sample to sample[9–11]. This approach allows us to take static snapshots of the nucleation process by ssNMR experiments under DNP conditions. Technology to achieve rapid freeze quench (RFQ) to vitrify solutions without glassing agents is not yet commercially available for ssNMR studies, but home-built RFQ setups have been used.[10,12–14] The main challenge with an RFQ setup is the several tens of μL volume typically required for a ssNMR magic angle spinning (MAS) sample. Wilson et. al demonstrated that spraying the sample into chilled isopentane can decrease the vitrification time and minimize the concentration of cryoagents to 20% glycerol[15]. However, commercial ssNMR Bruker sapphire rotors with capped bottoms are not compatible with this approach as it is not easily feasible to separate the isopentane solvent from the sample. Alternate design setups include spraying small droplets of sample onto a cryogenically cooled copper plate, however ample sample collection and functional rotor packing still leaves room for major improvements[14]. With the increasing popularity of DNP-NMR and electron paramagnetic reconance (EPR) studies of vitrified samples, we believe that technology for achieving rapid freeze quench without glassing agents will become available.

Phosphates are ubiquitous within the biologic and industrial materials fields, serving as essential energy storage vehicles and structural units[16**?** –19]. Phosphates have also recently

been shown to exhibit liquid-like clusters in solution, presenting additional complexity to understanding the growth of phosphate-containing structures[20,21]. The nonclassical nucleation of calcium phosphate clusters as the precursors to bone formation has been observed within seconds at concentrations which are only accessible to NMR enhanced by dissolution DNP[8], resulting in inadequate time for structural analysis. Sample vitrification and the extraction of the number of coupled ^{31}P nuclei at various early stage time points would allow for monitoring PNCs and the evolution of calcium phosphate phase formation. The feasibility of spin counting in vitrified solutions under DNP conditions for ^{31}P species should be relevant to the many biological and chemical processes that use phosphate containing species as structural building blocks or energy sources. Our studies show the feasibility of DNP-enabled spin counting and can be expanded to any spin $\frac{1}{2}$ system in the future.

In the case of calcium phosphate, understanding the assembly and growth mechanism(s) of phosphate clusters is the first step in elucidating the structure and evolution of the various species formed. In this effort, the most rudimentary question is how many phosphorous atoms are correlated in the species formed along the phosphate nucleation growth pathway? This question can be answered by counting the number of coupled ^{31}P spins with multiple quantum NMR (MQ-NMR) spin counting (MQ-SC)[?]. In fact, MQ-SC might be the only technique available to count the number of coupled nuclei in soluble, small clusters of magnetically indistinct environments. Notably, while spin counting has been utilized to characterize amorphous[22–25] or crystalline solids[26?–31], it has never been applied to characterize the structure of soluble assemblies and clusters in solution upon vitrification.

Spin counting is an experimental NMR technique where Multiple Quantum Coherences (MQCOs) are created between dipolar or J-coupled nuclear spins. In such experiments, a coherence is defined as a multiple spin transition (forbidden but made allowable by spin-spin coupling) from different ground states to the same excited state at the same time and with the same phase[32]. The number of neighboring nuclei, the distances between them and the uniformity of their spatial arrangements determine the number of MQCOs one

can detect[?], along with the mode of MQCO excitation[?]. While traditional MQ-NMR employs standard phase cycling to select each coherence order in a separate experiment, MQ-SC experiments increment the phase of either the excitation or reconversion block, allowing for different coherence evolution in a single experiment[?] (Figure S1). MQ-NMR spin counting still requires multiple experiments to extract the individual frequencies of each coherence order, which is either done via a 2D experiment with time-proportional phase incrementation, in which the excitation pulse phase increment is proportional to the t_1 evolution or via a pseudo 2D experiment with the excitation pulse phase incremented and directly detected in the t_2 dimension[33?]. MQ-SC has been performed on crystals[26? –31], liquid crystals[22,34], minerals[35? –38], catalysts/zeolites[38–46], glasses[23], molecules[47–49], amorphous semiconductors[22,24,25], hybrid materials[50], thin films/polymers[51–54], diamond surfaces[?], and peptides/proteins[55–59], all under static or varying MAS rates with various nuclear spins (S=1/2 and 3/2[60,61]) and employing zero quantum, single quantum, double quantum (DQ), or triple quantum (TQ) propagators. The aforementioned extensive history of successful spin counting experiments demonstrates it as a reliable technique, however MQ-SC under DNP conditions of solution species vitrified in a frozen matrix has never been performed by any study reported to date to our knowledge. Our critical case study provides an avenue for future studies of solution intermediate states, showing the feasibility of quickly analyzing these otherwise indistinguishable spectroscopic signatures, even when suffering from low sensitivity.

Here, we present novel ^{31}P NMR spin counting studies of both powdered and vitrified phosphate-containing samples, for which we have extracted the minimum number of dipolar coupled spins via the creation of multiple even and odd quantum coherence orders[62] using the SR2$^1_8$ pulse sequence (see Figure S1 and Listing 2, Supporting Information)[28,63], where the overall phase of the excitation block is incremented in a pseudo 2D mode to extract the MQCOs. The SR2$^1_8$ pulse sequence is an R-symmetry based double quantum recoupling sequence[64] which works with a low radio frequency power requirement equal to half the

spinning frequency, hence permitting longer recoupling times. The $SR2_8^1$ pulse sequence is a non-gamma encoded[65] sequence and is a super cycled version of $R2_8^1$, described as $\pi/2$-pulse-sandwiched $R2_8^1R2_8^{-1}$ pulse sequence which has a duration of 16 rotor periods as shown in Figure S1. Longer recoupling times are required to generate the higher multiple quantum coherences. We also present a novel method for analyzing MQ-SC data, for which we extract individual frequencies of the spin transitions using knowledge based fitting with n (integer) multiple of cosine waves, allowing for more physically meaningful extraction of the minimum bound of coupled nuclear spins when compared to the traditional Fourier transform which can generate nonphysical frequencies.

In this study, we present proof of concept applications of MQ-SC experiments on powdered and their respective vitrified solution species counterparts, along with a novel calcium phosphate time stabilized prenucleation system. We focus first on both discrete and extended ^{31}P dipolar coupled systems for spin counting studies, demonstrated respectively for molecular adenosine triphosphate (ATP), amorphous calcium phosphate (ACP) and crystalline hydroxyapatite (HAp) ($Ca_5(PO_4)_3OH$), where ACP is an amorphous precursor to HAp in the crystallization pathway of calcium phosphate[66]. We then discuss experiments with a modified simulated body fluid (mSBF)[67,68] shown to contain calcium phosphate prenucleation clusters[7], which spontaneously phase transform and aggregate to form ACP[69]. We have prepared our samples according to common dynamic nuclear polarization (DNP) sample preparation practices. DNP typically utilizes stable bi-radicals (in our study, AMUPol) by saturating the EPR resonance of a sub-population of the bi-radicals via microwave irradiation to transfer polarization to nuclear spins of the solvent, resulting in significant signal enhancements[70]. All samples were prepared for vitrification in a solution of 6:3:1 parts by volume glycerol-d8, D_2O, and H_2O respectively with 10 mM (Figure 1 and 2) / 6.67 mM (Figure 3) AMUPol (referred to as DNP juice). Samples were first prepared in 100 % H_2O or 75/25 % D_2O/H_2O (see Supporting Information Materials Section and Figures 2B and S11 for methodology), then the bi-radical AMUPol and glycerol-d8 were subsequently added.

Figure S18 displays the ^{31}P signal both with and without DNP, illustrating the crucial need for DNP at these low concentrations.

For our study, we disregard the potential impact of the paramagnetic polarizing and glassing agents on the reaction pathway, given that the chemical shift between powdered and vitrified samples closely align for HAp, ACP, and ATP samples (Figure S5, B and C). The effect of glycerol on the non-classical growth pathway to form ACP from modified simulated body fluid (mSBF) samples containing PNCs cannot be verified given that there is no powder sample for comparison. We found that glycerol can increase the solubility of ACP at lower calcium and phosphate concentrations (verified by DLS, solution NMR, and ssNMR not shown in this paper), but the systematic and mechanistic study of the role of glycerol in modulating the equilibrium or kinetics of the non-classical growth pathway of ACP is outside the scope of this study[14,71]. Here, we only focus on the question whether DNP-enhanced NMR of manually plunge frozen mSBF samples, en route to ACP solids, can capture vitrified intermediate species in solution state and whether ^{31}P MQ-SC can identify one or more of these species to be PNC candidates.

MQ filtering efficiencies represent the ability for a pulse sequence to filter out all spin flip transitions other than the specific MQ transition. We find that the large chemical shift anisotropy (CSA) of ^{31}P nuclei in nonsymmetric molecular systems such as ATP (Figure S7a)[72] reduces the DQ filtering efficiency of the $SR2^1_8$, $R14^6_2$, and SPC-5 pulse sequences, with $SR2^1_8$ expected to be minimally sensitive to CSA since it is a super cycle version of $R2^1_8$ and capable of delivering a theoretical maximum efficiency of around 50 %. Under our experimental conditions, the DQ filtering efficiencies for powdered ATP samples were found to be 3.12, 3.125, and 5.40 % when using the $SR2^1_8$, $R14^6_2$, and SPC-5, respectively. In contrast for powdered HAp, the experimentally measured DQ filtering efficiencies were found to be 45, 34.5, and 41.1 % when using the $SR2^1_8$, $R14^6_2$, and SPC-5, respectively. Based on these results, we decided to continue our experiments on each sample with $SR2^1_8$ to achieve DQ and TQ filtering efficiencies (Supporting Information Listing 1). We independently found an

optimal DQ and TQ excitation time of 1.6 ms (3.2 ms mixing time) at a MAS frequency of 10 kHz for each ^{31}P powdered and vitrified sample. Crystalline HAp exhibits an extended spin lattice network with a DQ/TQ filtering efficiency of 45/6.56 % at room temperature and a DQ efficiency of 38 % at 100 K in DNP juice. Powdered ACP was found to have a slightly lower DQ filtering efficiency of 43 % at room temperature and a DQ/TQ filtering efficiency of 33.4/3.7 % at 100 K in DNP juice. ATP suffered from low DQ and TQ filtering efficiencies of 3.12/0.28 % when powdered at room temperature and 1.3/0.4 % at 100 K (20 and 40 mM ATP in glycerol-d8 DNP juice). The mSBF sample suffered from low overall signal, thus not allowing for TQ filtering signal even after 1024 scans. However DQ filtering efficiency was determined to be 6.25 % at 100 K in DNP juice. Vitrified sodium monophosphate control sample (Figure S10) exhibited no DQ filtering signal as expected, even after 512 scans. The refocusing of the CSA will be sensitive to magic angle frequency instabilities since the $SR2_8^1$ is a non-gamma encoded sequence. We carried out the numerical simulations mimicking the MAS fluctuations to find out its effect on DQ efficiency with and without CSA (shown in the Figure S7b). In both cases of CSA and non-CSA, the DQ signal intensity did not change with a fluctuation rate of $\pm$ 5 Hz, however, when the fluctuation was increased to $\pm$ 20 Hz, then DQ signal intensity was varied for both cases. During our experiments, the MAS fluctuation was around $\pm$ 5 Hz, indicating that the signal intensity variation was minimal as explained by simulation results.

Depending on the sample and experimental conditions, both intramolecular and intermolecular coherent spins can be probed by MQ-SC. In simulations of MQ-SC experiments (Figure S8), up to 6 coherence orders can be seen in a linear chain of ^{31}P spins separated at a distance of 2.5 Å in between. We optimized the excitation time at a MAS frequency of 10 kHz (Figure S13) with the DQ filtered even order MQ-SC pulse sequence in order to maximize the extracted MQCOs, and found an excitation time of 8 ms (mixing time of 16 ms) to be optimal across all different ^{31}P nuclei containing powdered samples and their respective vitrified counterparts (Figure 1 and 2). However, the mSBF sample (which suf-

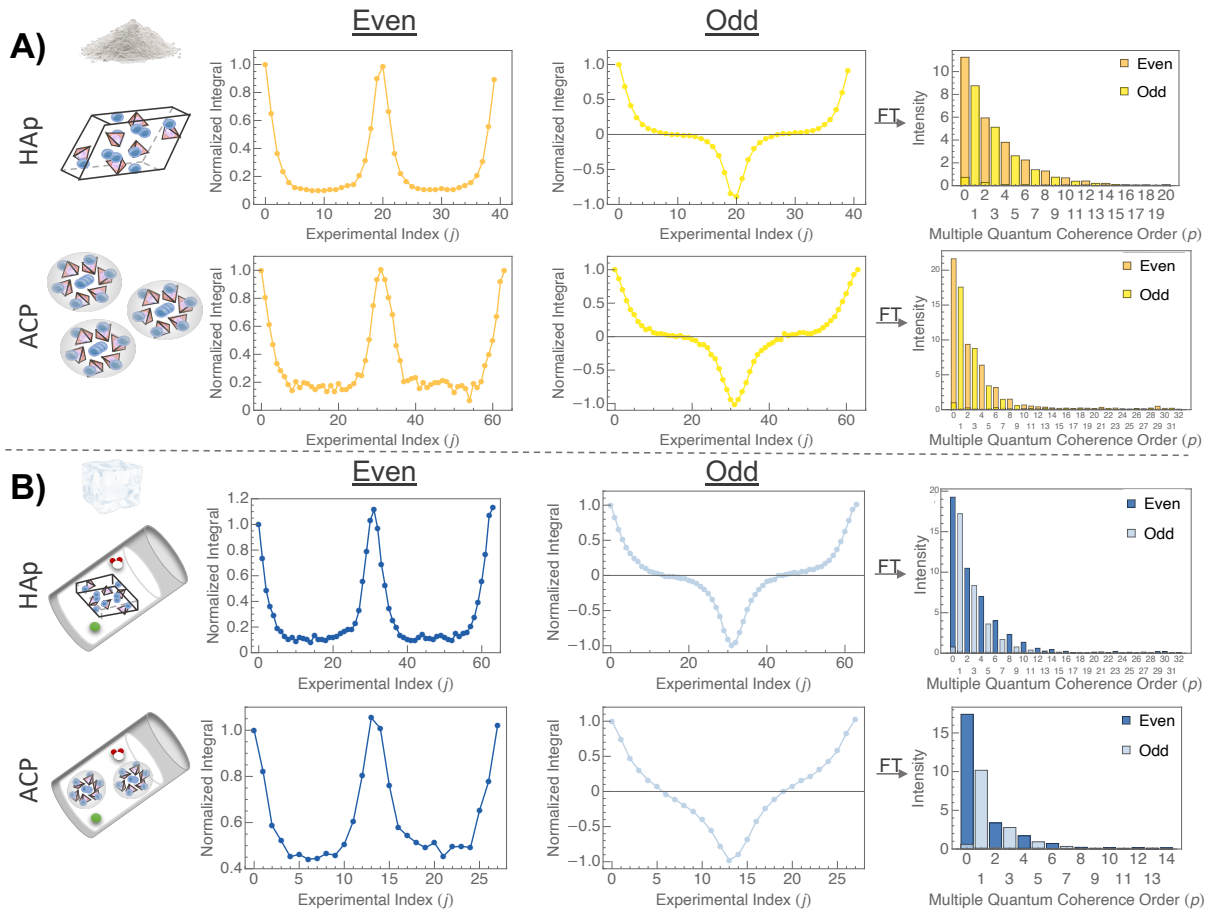

Figure 1: Even and odd spin counting profiles and subsequent Fourier transformed MQCO (p) profiles at 10 kHz MAS and 8 ms excitation time for HAp (unit cell coordinates from reference 73) and ACP at A) Room Temperature B) 100 K Vitrified Conditions in DNP juice using $SR2_8^1$ pulse sequence (Figure S1) and a relaxation delay of 5 s. The x-axis of the spin counting profiles is represented as experimental index (j), where phase is incremented at each index by $360°/(j)$. All spin counting profiles' integrals were normalized to the integral of the first experiment ($j = 0$). The SC profiles represent the summation of all excited MQCO transition frequencies, which are extracted and discretized via Fourier transform into MQCO profiles.

fered from low DQ filtering signal) had an optimal excitation time of 4.8 ms (9.6 ms mixing time) for the middle CS environments, as determined by MQ-SC experiments (Figure 3C and S16). We ensured that the recycle delay and excitation times were set appropriately based on experimental relaxation parameters (See Figures S13 and S14). We employed these optimal parameters for spin counting experiments utilizing the $SR2_8^1$ pulse sequence to count the even and odd coherence orders (Figure S1). When examining a MQ-SC profile in order to determine the minimum number of clustered spins, any odd coherences shown for the even order MQ-SC profile (and vice versa) can be attributed to experimental noise and MQCO leakage caused by imperfect filtering of the double quantum recoupling sequences (Figure S8). The zero order coherence for even MQCO profiles is attributed to z-magnetization of the spins.

We show in Figure 1 signal integral of each MQ-SC experiment as a function of the excitation block pulse phase and the resulting Fourier transformation of this MQ-SC profile yields the amplitude for the MQCO for each phosphate-containing species, in powder form at room temperature (A) and vitrified at 100 K in DNP juice (B). We find for HAp even and odd coherence orders up to 14 and 13, respectively, at room temperature (Figure 1A). When samples are dissolved into DNP juice and characterized at 100 K, we find the measured coherences orders to be comparable at 14 and 11 for the same excitation time (Figure 1B). Similarly, we find for ACP even and odd coherence orders up to 10 and 9 at room temperature, and 8 and 7, respectively when dissolved into DNP juice, vitrified and measured at 100 K for the same excitation time. While excitation efficiency decreases with the increasing order of MQ transitions[74] and is further limited by pulse imperfections[75] (Figure S22), CSA relaxation (Figure S7a), and total spin concentration, the loss of coherence orders at 100 K is attributed to a shorter T_2 relaxation time of the vitrified sample compared to room temperature. Shorter T_2 will result in shorter recoupling times and the inability to excite higher order MQCOs of species with partially averaged out dipolar couplings, thus limiting the total intensity achievable for each individual MQCO. This higher MQCO truncation is

further exacerbated by individual n-quantum transition T_2 relaxation, which has been shown with EPR MQ-SC to decrease with higher orders[76].

In order to scale down concentration and molecular size, we next examined ATP. The conventional method of Fourier transforming the spin counting profile generated MQCOs of 2 for the even spin counting profile (Figure S9) and 1 and 3 for the powdered ATP odd spin counting profile (Figure S11) across all three alpha, beta, and gamma phosphorous chemical shift environments at room temperature. However this method also generated additional MQCOs of 2, 4, and 5 for the odd spin counting profile with comparable magnitudes. The Fourier transformation technique produces all frequencies, thus results in all possible MQ-COs. We find and will show that this analysis procedure is not accurate in extracting the lower bound of frequencies present in the MQCO profile (highest visual MQCO). Instead we employed a method of multi-cosine function fitting where the spin counting profile takes the form of multi-cosine waveforms as explained by the Average Hamiltonian Theory of Olyer and Tycko[77], further explained in the Supporting Information Section VI.

Before applying this innovative fitting method to ATP, we tested the method on our room temperature ACP sample from Figure 1 to demonstrate that our new method works consistently and at the minimum reproduces the results obtained by the Fourier Transform technique. In Figure S19, MQCOs of 7 and 8 can be seen above the error bars using the multi-cosine fitting method for odd and even spin counting profiles respectively. In addition, we applied the same fitting method by considering only even or odd frequencies with respect to the even or odd spin counting profile, with a maximum integer multiples of 8 or 7 respectively. Remarkably, the fitting convergence was identical when both even and odd frequencies were considered. These extracted MQCOs are similar to the conventional Fourier transform technique which extracted 9 and 10 respectively. We conclude that the fitting method with integer multiple of cosine waves provides a more dependable lower bound of MQCOs above the error value.

We adopted the same multi-cosine waveform fitting method to extract the MQCOs

present in ATP spin counting profiles. High CSA in ATP made extracting the MQCOs more challenging using Equation 5 in Supporting Information Section VI. To account for imperfect time reversal and high CSA values, we introduced the phase shift in Equation 6 in the limit of cosine approximation value close to zero. Odd spin counting experiments on ATP yielded the expected coherence orders of 3 for the alpha, beta, and gamma phosphorous chemical shift environments at room temperature (Figure 2B, top half) above the error value by considering all frequencies 0 through 3 in the fitting procedure based on Equation 6 in Supporting Information Section VI. When cosine frequencies 4 and 5 were considered in Figure S20, they did not exceed the error. This observation is consistent with the selective buildup of only intramolecular coherence orders in ATP and was validated by a sodium phosphate control sample (Figure S10). Due to a combination of factors, including high CSA (Figure S15) and imperfection in the glassing matrix, the MQCO extraction from ATP under DNP conditions was more challenging than that from HAp and ACP, as will be discussed in the following paragraph. We can currently conclude that as the number of intramolecular phosphate bonds and long range order increases, the extracted MQCOs increase, as seen with increasing MQCOs in the order of ATP, ACP, and HAp. We find that the process of vitrification does not drastically affect the extracted coherence orders and any loss of MQCO can be attributed to a decreased signal to noise ratio due to shortened T_2 relaxation at low temperature. We also find that by using multi-cosine curve fitting method instead of the Fourier transform, we can more confidently determine the lower bound of extracted MQCOs.

The extraction of a coherence order of 3 for ATP in DNP juice at 100 K was challenging. We explored the effect of different solvents and vitrifying methods to mitigate the MQCO dampening effects seen with MQ-SC of ATP. We first explored utilizing DMSO instead of glycerol as a glassing solvent in a 77:17:6 DMSO$-d_6$:D_2O:H_2O ratio[79], which prolonged the long T_2 component from 12.95 ms (in glycerol) to 13.56 ms (in DMSO) (Figure S14). We observed a minimum of 3 MQCOs across the alpha, beta, and gamma chemical shift environments for ATP in DMSO when we applied cosine frequencies of 1 through 3 (Figure

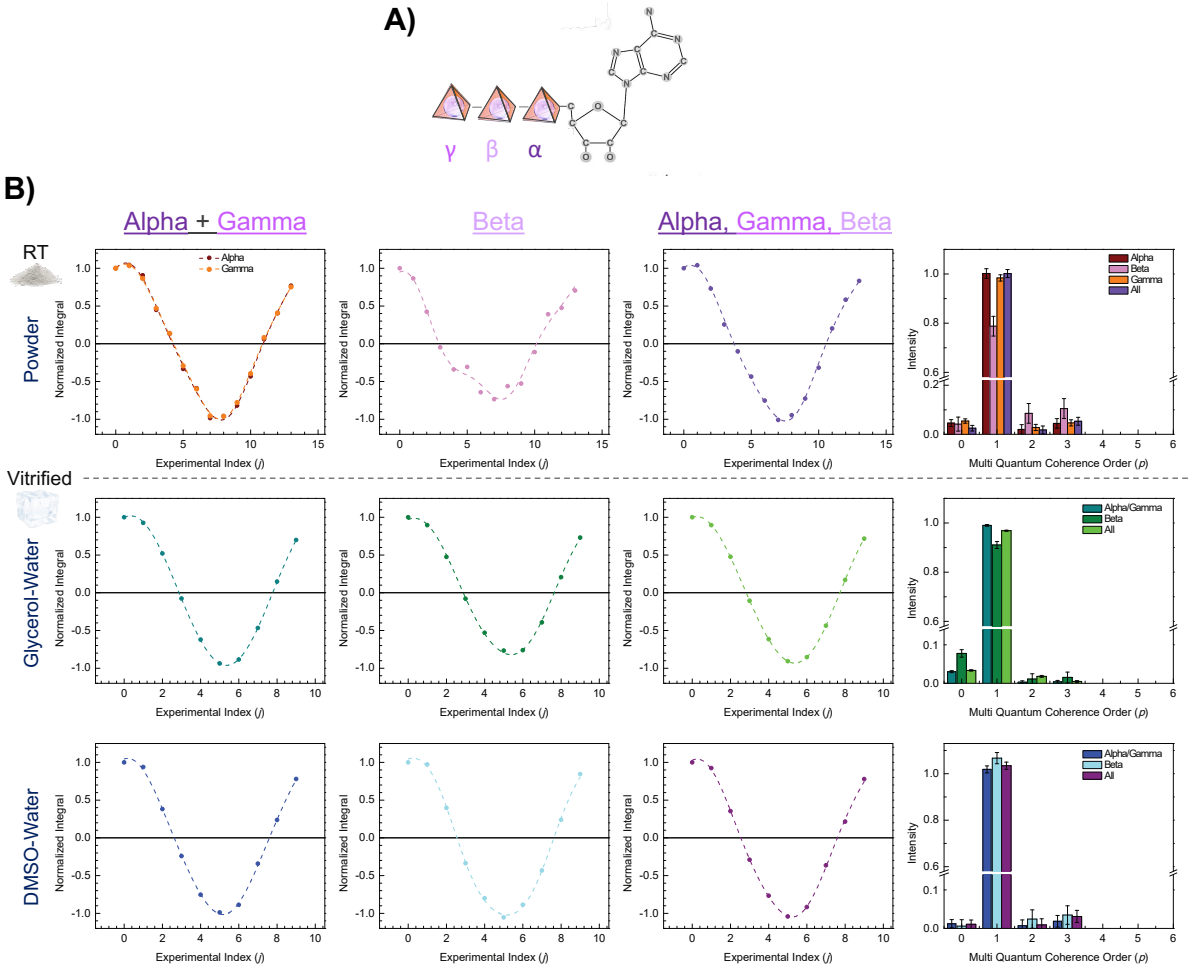

Figure 2: A) ATP labeled PO_4 sites γ, β, and α, equivalent to Q1, Q2, and Q1 respectively[78]. B) Odd spin counting profiles and MQCO charts extracted from multi-cosine function curve fitting (SI Section VI) with frequencies 0 through 3 for a room temperature powdered and two 100 K vitrified ATP samples in glycerol and DMSO at 10 kHz MAS and 8 ms excitation time. 20 mM ATP vitrified samples (final concentrations in DNP juice) were prepared in the dissolution order of AMUPol, H_2O, D_2O, glycerol-d8/DMSO-d6, ATP. ATP in DMSO exhibited a final pH of 5.88, while ATP in glycerol was pH corrected as a final step with 1M NaOH to 10. Each chemical shift range assigned to individual PO_4 sites was chosen based upon ^{31}P spin connectivity determined in Figures S5 and S6. All experiments were taken with a relaxation delay of 6 s. Monophosphate breakdown can be viewed in Figure S10. Conventional SC analysis, along with additional solvent comparisons, can be viewed in Figure S11 and S20.

2B). With the Fourier transform method, we see up to 5 which may be attributed to intermolecular clustering, however more data points are necessary for analysis with the new fitting method. We returned to the glycerol:D_2O:H_2O mixture since DMSO potentially was inducing clustering. When using the glycerol:D_2O:H_2O mixture, we tested the effects of the order of mixing solution constituents, ATP concentration, and vitrification procedure to minimize clustering and to push the equilibrium towards deprotonating the phosphate O-H bonds (Figure S11). These modifications resulted in an elongated T_2 from 8.32 ms to 17.92 ms. Different conditions varied T_2 relaxation (Figure S14). Among them, a sample of 20 mM ATP in glycerol showing a T_2 of 12.95 ms resulted in 3 weakly visible MQCOs when we applied cosine frequencies of 1 through 3 (Figure 2B, top). We took this sample and exposed it to an electric field of 7 kV for 3.5 minutes (Figure S11B), then immediately plunged the entire system with the power source still on (ensuring no loss of orientation) into liquid nitrogen for vitrification and transferred the sample to the spectrometer under cryogenic temperatures. This setup was inspired by a study from Tang et al.[80] to align the aromatic rings of ATP with an electric field that led to an energetically preferred π-stacking configuration. The hypothesis was that the stacking alignment would decrease the CSA of ATP. The experimental results show that the CSA increased for some phosphate environments and decreased for others in a nontrivial manner (Figure S15). Still, the third MQCO became more visible in every CS environment after the exposure of the ATP solution to an electric field. It is clear that future applications of this method to ^{31}P species with lower CSA will prove more fruitful. In fact, an ongoing study in our group on the assembly of phosphorylated proteins show that the minimal CSA of phosphate groups makes spin counting of a high MQCO of a vitrified protein fibril feasible. We will next showcase a proof of principle study that achieves the detection of transiently formed phosphate prenucleation clusters upon vitrification in solution by DNP-enhanced MQ-SC.

In the pursuit of a system with a prenucleation cluster which would likely exhibit less CSA[81] than molecular ATP, we set out to arrest calcium phosphate prenucleation clusters.

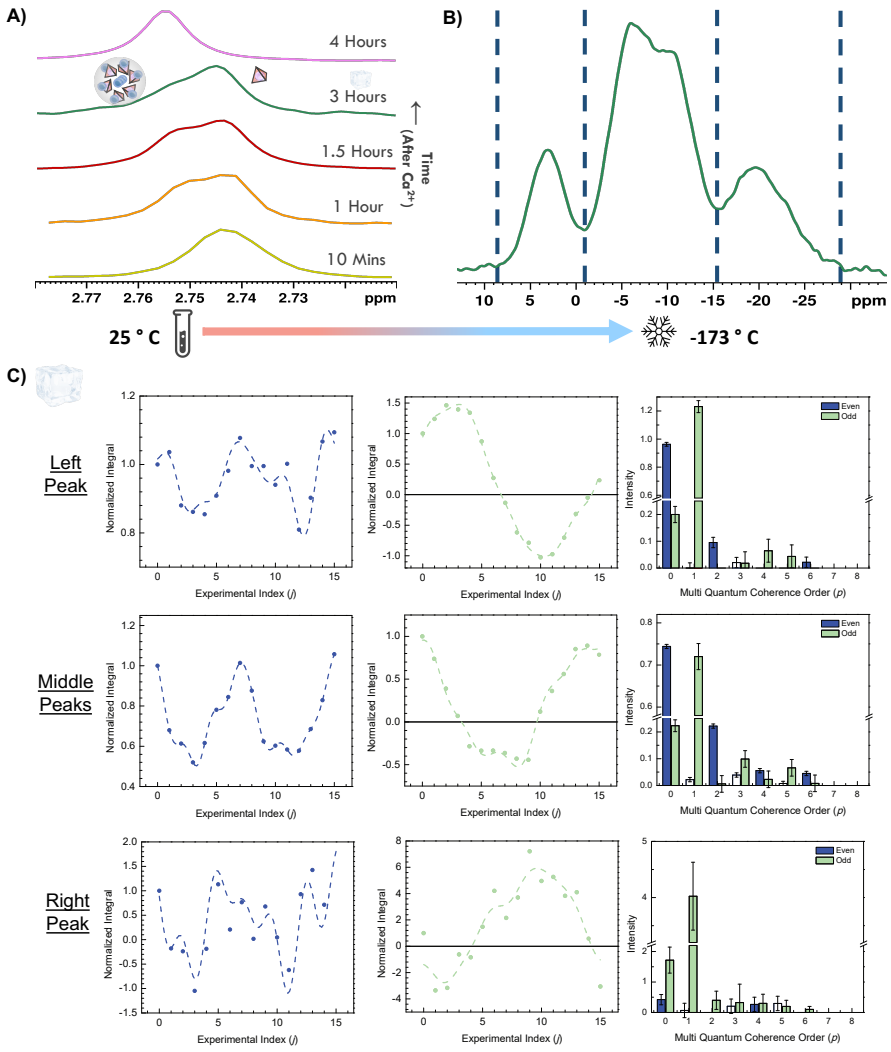

Figure 3: MSBF solution (A) and vitrified sample (B). In A), direct ^{31}P solution NMR time evolution of mSBF solution in 90 % water and 10 % D_2O by volume, with total solution concentration of 1.32 mM and 0.6487 mM phosphate and calcium respectively (other salts found in Supporting Information Materials). These spectra were chemical shift corrected to a phosphoric acid coaxial insert sample. An aliquot was taken at 3 hours after addition of calcium for DNP juice preparation and subsequently vitrified, found in part B. When left to react over a time period of 24 hours, the peak continues to shift left and sharpen, likely forming HAp. In B), the ^{1}H to ^{31}P CP 1D spectra of vitrified mSBF (referenced to phosphoric acid) in 60 % volume glycerol with a 1:9 total solution volume dilution factor, resulting in final concentrations of 0.147 mM phosphate and 0.072 mM calcium (complete preparation in Supporting Information Materials). The ^{31}P T_1 relaxation exceeded 100 s. The three blue regions are analyzed in part C. (C) Spin counting of vitrified mSBF sample with multi-cosine function curve fitting methodology (conventional SC analysis found in Figure S12) using a mixture of frequencies 0 through 6 for both even and odd MQ-SC data sets (Supporting Information Section VI). For each even or odd experiment, the corresponding extracted MQCOs not filled in represent the opposite integer noise. Even and odd SC experiments were taken with a relaxation of 5 s and optimal excitation time of 4.8 ms at 10 kHz MAS. The right chemical shift environment suffered from low signal for even and odd SC, even at 256 and 512 scans respectively.

The nucleation pathway for calcium phosphates is an important topic that many scientists are interested in, but also grappling with. As a result, there is no agreed upon method to control the nucleation pathway to date. We have experienced ourselves that a multitude of factors influence this pathway in unexpected ways, such as the order of mixing components and the angle at which one pipettes. We decided to reproduce the calcium phosphate clusters studied by Epasto, et al[7], however due to the inherent delicate nature of these processes, a few small modifications of the Kurzbach sample preparation method were necessary to observe PNCs under our laboratory conditions (Supporting Information Methods). Our replicate mSBF ^{31}P solution NMR experimental conditions (Figure 3A) exhibit a faster transition timescale, where the splitting of the ^{31}P solution NMR lineshape offers evidence for the formation of approximately 2 nm size PNCs exchanging with free dissolved phosphate according to Kurzbach and coworkers[7]. We could not perform DLS on our mSBF recipe due to the presence of HEPES agent, which obscures other similar or smaller sized particles around 1 nm. It is well known among groups that study these processes that PNC formation is a kinetic process that is highly sensitive to any experimental variation, including the choice of buffer, temperature, certainly the exact composition of the mSBF and even the order and method of salt mixing. Further complicating interpretation, the solution ^{31}P NMR chemical shift of monophosphate salt is dependent on the total ionic strength of the solution in a nonlinear relation (likely due to effects such as water hydration structure and extent of hydration), while conversely related to the pH and temperature[20,21] of the solution in a linear relation (Figure S17). Given the complexity of these processes that require more scrutiny, the elucidation of PNC formation pathways is beyond the scope of our study. Instead, we present a proof of principle study of MQ-SC under DNP conditions of PNCs to showcase the feasibility of such an approach, especially of solution state clusters in vitrified solution.

We were able to extract an approximate ^{31}P solution NMR T_2 relaxation for the splitting time point of 6.14 ms and a T_1 of 7.4 (monoexponential fit) 95% 7.94 s and 5% 0.47 s (biexponential fit) with an error of 0.5 s. We arrested the solution at three hours when there

was explicit NMR splitting that had been stable across a formation time of a few hours, by adding AMUPol already dissolved in D_2O, then glycerol-d8, and lastly plunging the sample in liquid nitrogen. The resulting final vitrified sample consisted of 0.147 mM phosphate and 0.072 mM calcium total. A 1D ssNMR spectrum was acquired of this sample. Four distinct ^{31}P NMR chemical shifts appeared (Figure 3B). We completed even and odd spin counting experiments on this sample and analyzed these chemical shift environments (Figure 3C), where the middle peak two environments were combined into one due to their very closely overlapping chemical shifts. We extracted even ordered experimental minimum MQCOs of 2, 6, and 2 for the left, middle, and right peaks respectively with the conventional MQ-SC Fourier transform analysis (Figure S12), which agreed very closely with our multi-cosine fitting method extracted MQCOs of 2, 6, and 0. The odd spin counting experiments show MQCOs of 1, 5, and 1 for the left, middle, and right peaks respectively for both fitting methods. Both odd and even spin counting experiments have different experimental noise levels due to acquiring disparate scans because of limited signal; noise levels for even and odd MQCO experiments should be extracted from the same experiment type. For an even MQ-SC experiment, one should examine the even experimental noise in the unfilled adjacent bar (dark blue for traditional Fourier transform method in Figure S12) for the odd coherence orders. The left peak exhibits a very small MQCO of 2 for all excitation times (Figure S14) and has significant overlap with the CS of monophosphate control sample. The right peak environment was difficult to distinguish from noise during analysis and as evidenced by the even and odd SC profile showing no discernible cosinusoidal shape or meaningful Fourier transform. This might be due to the presence of a significant population of isolated phosphates present, not enough scans acquired, or due to a different optimal excitation time of 3.2 ms / mixing time of 6.4 ms (Figure S16, MQCO of 2 is clearly extracted with conventional Fourier transform method). This middle merged peak environment has a T_2 relaxation of 14.17 ms (which is more than the experimental mixing time of 9.6 ms) and exhibits a lower CSA than most environments for ATP in DNP juice, and yielded an extracted

MQCO of a minimum of 6. Considering the MQ-SC results of model systems and fully formed HAp crystals and ACP solids, the observation of such a high and distinct MQCO of 6 is unexpected and significant. The results of different analysis methods are consistent in yielding a MQCO of 6; the incorporation of additional cosine frequencies 7 and 8 did not exceed their respective error bars (Figure S21). The species giving rise to MQCO of 6 could be small ACP solids or likely a calcium phosphate prenucleation cluster (or both due to the presence of two peaks), potentially even including the Posner cluster which is proposed to be made of six phosphate atoms[81–83]. These exploratory results can be expanded upon with further structural analysis in the future.

In summary, the successful counting of ^{31}P nuclei clustering in vitrified solutions provides a novel structural analysis approach to characterize nonclassical growth pathways that include pre-nucleation clusters as intermediate species. In the future, these MQ-SC experiments can be optimized to better resolve the higher order coherences using finer phase increments to better resolve their higher precession frequencies compared to that of lower order coherences. It should be possible to see a more distinct transition from higher coherence orders that are present vs those below noise levels to figure out the upper bound quantum number by sampling the precession frequencies with increasingly finer phase increments. MQ-SC might be one of the few techniques that can identify the formation of clusters made of the same species, here phosphates, that do not have distinguishable spectroscopic signatures between the coupled species. For clusters that cannot be isolated and/or are too small or with too little contrast to be captured by electron microscopy or various light scattering techniques, MQ-SC might in fact be the only approach to identify the minimal number of coupled phosphates in the cluster. MQ-SC is not a perfect experiment for ultimate quantification, but when it comes to a cluster of species with identical signal in solution state, there is no good alternative option. We have shown a great improvement in the method for analyzing MQ-SC data; by using more catered multi-cosine fitting, improved confidence in the minimum bound, highest visual MQCO can be achieved. In future studies, performing

spin counting experiments on prenucleation cluster species at lower concentrations than as found in this paper would require conducting more scans. In this study we showed that increasing the molecular order increased the measured MQCOs for both powdered and vitrified solutions. Asymmetric molecular systems may require additional sample preparation optimization under vitrified conditions in order to mitigate CSA relaxation effects, such as electric field exposure for aromatic systems as demonstrated here. We show that one can go down to sub milimolar concentrations for a proposed calcium phosphate prenucleation cluster and still extract an MQCO order of 6. MQ-SC opens the door for extracting quantitative information at newfound atomic-scales in dynamic systems. Spin counting experiments can be applied in the future to test various nonclassical growth models, such as further examination of the calcium phosphate nucleation pathway with simplification of our simulated body fluid recipe. Shedding light on calcium phosphate assembly will pave the path for future bone and biomimetic material technologies and potentially identify a source of mammalian information storage[81,84].

Acknowledgement

MSN and SH thank Alexej Jerschow for helpful discussions on the feasibility of MQ-SC under DNP conditions and Manisha Patel for being a part of the Quantum Brain team and supporting experimental work of this study. MSN and SH also would like to thank Dennis Kurzback and Ludovica Martina Epasto for extensive discussion on mSBF reproduction, exchanging protocols, and comparing results. We learned that the process is inherently delicate and complex, needing a better mechanistic understanding. MSN, JS, RC, and MP thank the Heising-Simons Foundation for support of the study of ACP formation. MSN thanks the National Science Foundation (NSF) Graduate Research Fellowship under Grant No. 1650114 for support, and RC and SJ thank the NSF for support of DNP method developments under Award No. CHE CMI 2004217. SH was also supported by the National Institutes of Health

under Award No. R35GM136411 for the DNP studies of biomolecules. This work made use of the MRL Shared Experimental Facilities supported by the MRSEC Program of the NSF under Award No. DMR 1720256; a member of the NSF-funded Materials Research Facilities Network. MSN, JSS, and SH acknowledge the support of NSF Major Research Instrumentation award, MRI-1920299, for solution magnetic resonance instrumentation.

Supporting Information Available

Supporting Information Available: Additional experimental details, materials, and methods, including pulse sequences and simulation results is available free of charge via the Internet at http://pubs.acs.org.

References

(1) Cölfen, H. Nonclassical Nucleation and Crystallization. *Crystals* **2020**, *10*, 1–3.

(2) Yang, X.; Wang, M.; Yang, Y.; Cui, B.; Xu, Z.; Yang, X. Physical Origin Underlying the Prenucleation Cluster Mediated Nonclassical Nucleation Pathways for Calcium Phosphate. *Phys. Chem. Chem. Phys.* **2019**, *21*, 14530–14540.

(3) Jiao, K.; Niu, L.-N.; Ma, C.-F.; Huang, X.-Q.; Pei, D.-D.; Luo, T.; Huang, Q.; Chen, J.-H.; Tay, F. R. Complementarity and Uncertainty in Intrafibrillar Mineralization of Collagen. *Adv. Funct. Mater.* **2016**, *26*, 6858–6875.

(4) Gebauer, D.; Wolf, S. E. Designing Solid Materials from Their Solute State: A Shift in Paradigms toward a Holistic Approach in Functional Materials Chemistry. *J. Am. Chem. Soc.* **2019**, *141*, 4490–4504.

(5) Juramy, M.; Mollica, G. Recent Progress in Nuclear Magnetic Resonance Strategies for

Time-Resolved Atomic-Level Investigation of Crystallization from Solution. *Current Opinion in Colloid & Interface Science* **2023**, *63*, 1–20.

(6) Cerreia-Vioglio, P.; Thureau, P.; Juramy, M.; Ziarelli, F.; Viel, S.; Williams, P. A.; Hughes, C. E.; Harris, K. D. M.; Mollica, G. A Strategy for Probing the Evolution of Crystallization Processes by Low-Temperature Solid-State NMR and Dynamic Nuclear Polarization. *J. Phys. Chem. Lett.* **2019**, *7*, 1505–1510.

(7) Epasto, L. M.; Georges, T.; Selimović, A.; Guigner, J.-M.; Azaïs, T.; Kurzbach, D. Formation and Evolution of Nanoscale Calcium Phosphate Precursors under Biomimetic Conditions. *Anal. Chem.* **2021**, *93*, 10204–10211.

(8) Weber, E. M. M.; Kress, T.; Abergel, D.; Sewsurn, S.; Azaïs, T.; Kurzbach, D. Assessing the Onset of Calcium Phosphate Nucleation by Hyperpolarized Real-Time NMR. *Anal Chem.* **2020**, *92*, 7666–7673.

(9) Leavesley, A.; Wilson, C. B.; Sherwin, M.; Han, S. Effect of Water/Glycerol Polymorphism on Dynamic Nuclear Polarization. *Phys. Chem. Chem. Phys.* **2018**, *20*, 9897–9903.

(10) Jeon, J.; Thurber, K. R.; Ghirlando, R.; Yau, W.-M.; Tycko, R. Application of Millisecond Time-Resolved Solid State NMR to the Kinetics and Mechanism of Melittin Self-Assembly. *PNAS* **2019**, *116*, 16717–16722.

(11) Baudot, A.; Alger, L.; Boutron, P. Glass-Forming Tendency in the System Water–Dimethyl Sulfoxide. *Cryobiology* **2000**, *40*, 151–158.

(12) Kaufmann, R.; Yadid, I.; Goldfarb, D. A Novel Nicrofluidic Rapid Freeze-Quench Device for Trapping Reactions Intermediates for High Field EPR Analysis. *J. Mag. Reson.* **2013**, *230*, 220–226.

(13) Schmidt, T.; Jeon, J.; Okuno, Y.; Chiliveri, S. C.; Clore, G. M. Submillisecond Freezing Permits Cryoprotectant-Free EPR Double ElectronElectron Resonance Spectroscopy. *Chem Phys Chem* **2020**, *21*.

(14) Nowotarski, M. S. Elucidating Phosphate Cluster Formation Mechanisms through Nuclear Magnetic Resonance - Vitrification Methods & Design of Rapid Freeze Quench. *University of California, Santa Barbara Dissertation* **2023**,

(15) Wilson, C. B.; Tycko, R. Millisecond Time-Resolved Solid-State NMR Initiated by Rapid Inverse Temperature Jumps. *J. Am. Chem. Soc.* **2022**, *144*, 9920–9925.

(16) Dzeja, P. P.; Terzic, A. Phosphotransfer Networks and Cellular Energetics. *J. Exp. Biol.* **2003**, *206*, 2039–2047.

(17) Blumenthal, N.; Posner, A. Hydroxyapatite: Mechanism of Formation and Properties. *Cal. Tis Res.* **1973**, *13*, 235–243.

(18) Schröder, H.; Kurz, L.; Müller, W.; Lorenz, B. Polyphosphate in Bone. *Biochem.* **2000**, *65*, 296–303.

(19) Wang, L.; Nancollas, G. H. Calcium Orthophosphates: Crystallization and Dissolution. *Chem. Rev.* **2008**, *108*, 4628–4669.

(20) Straub, J. S.; Nowotarski, M. S.; Lu, J.; Sheth, T.; Jiao, S.; Fisher, M. P.; Shell, M. S.; Helgeson, M. E.; Jerschow, A.; Han, S. Phosphates Form Spectroscopically Dark State Assemblies in Common Aqueous Solutions. *PNAS* **2022**, *120*, 1–10.

(21) Lu, J.; Straub, J. S.; Nowotarski, M. S.; Han, S.; Xu, X.; Jerschow, A. Spectroscopically Dark Phosphate Features Revealed by Chemical Exchange Saturation Transfer. *NMR Biomed* **2023**, *In Press*.

(22) Baum, J.; Pines, A. NMR Studies of Clustering in Solids. *J. Am. Chem. Soc.* **1986**, *108*, 7447–7454.

(23) Fayon, F.; Duée, C.; Poumeyrol, T.; Allix, M.; Massiot, D. Evidence of Nanometric-Sized Phosphate Clusters in Bioactive Glasses As Revealed by Solid-State 31P NMR. *J. Phys. Chem.* **2013**, *117*, 2283–2288.

(24) Petrich, M. A.; Gleason, K. K.; Reimer, J. A. Structure and Properties of Amorphous Hydrogenated Silicon Carbide. *Phys. Rev. B* **1987**, *36*, 9722–9731.

(25) Gleason, K. K.; Petrich, M. A.; Reimer, J. A. Hydrogen Microstructure in Amorphous Hydrogenated Silicon. *Phys. Rev. B* **1987**, *36*, 3259–3267.

(26) Tomaselli, M.; Hediger, S.; Suter, D.; Ernst, R. R. Nuclear Magnetic Resonance Polarization and Coherence Echoes in Static and Rotating Solids. *J. Chem. Phys* **1996**, *105*, 10672–10681.

(27) Ba, Y.; Veeman, W. S. Multiple-Quantum Nuclear Magnetic Resonance Spectroscopy of Coupled 1/2 Spins in Solids. Combination with Cross-Polarization and Magic-Angle Spinning. *Solid State Nucl. Magn. Reson.* **1994**, *3*, 249–269.

(28) Teymoori, G.; Pahari, B.; Viswanathan, E.; Edén, M. Multiple-Quantum Spin Counting in Magic-Angle-Spinning NMR via Low-Power Symmetry-Based Dipolar Recoupling. *J. of Magn. Reson.* **2013**, *236*, 31–40.

(29) Antzutkin, O. N.; Tycko, R. High-Order Multiple Quantum Excitation in 13C Nuclear Magnetic Resonance Spectroscopy of Organic Solids. *J. Chem. Phys.* **1999**, *110*, 2749–2752.

(30) Levy, D. H.; Gleason, K. K. Multiple Quantum Nuclear Magnetic Resonance as a Probe for the Dimensionality of Hydrogen in Polycrystalline Powders and Diamond Films. *J. Phys. Chem.* **1992**, *96*, 8125–8131.

(31) Bertani, P.; Raya, J.; Hirschinger, J. 19F/29Si Distance Determination and Heteronu-

clear Spin Counting Under Fast Magic-Angle Spinning in Fluoride-Containing Octadecasil. *Comptes Rendus Chimie* **2004**, *7*, 363–369.

(32) Sánchez, C. M.; Pastawski, H. M.; Levstein, P. R. Time Evolution of Multiple Quantum Coherences in NMR. *Physica B: Condensed Matter* **2007**, *398*, 472–475.

(33) Shykind, D.; Baum, J.; Liu, S.-B.; Pines, A.; Garroway, A. Phase-Incremented Multiple-Quantum NMR Experiments. *J. Mag. Res.* **1988**, *76*, 149–154.

(34) Gerasimowicz, W. V.; Garroway, A. N.; Miller, J. B. Multiple-quantum NMR in a Mixture of Liquid Crystals: Differential Coherence Development. *J. Am. Chem. Soc.* **1990**, *112*, 3726–3730.

(35) Cho, G.; Yesinowski, J. P. H and 19F Multiple-Quantum NMR Dynamics in Quasi-One-Dimensional Spin Clusters in Apatites. *J. Phys. Chem.* **1996**, *100*, 15716–15725.

(36) Mogami, Y.; Yamazaki, S.; Matsuno, S.; Matsui, K.; Noda, Y.; Takegoshi, K. Hydrogen Cluster/Network in Tobermorite as Studied by Multiple-Quantum Spin Counting 1H NMR. *Cement and Concrete Research* **2014**, *66*, 115–120.

(37) Cho, G.; P.Yesinowski, J. Multiple-Quantum NMR Dynamics in the Quasi-One-Dimensional Distribution of Protons in Hydroxyapatite. *Chem. Phys.Lett.* **1993**, *205*, 1–5.

(38) Gerstein, B. C.; Pruski, M.; Hwang, S.-J. Determination of Proton Densities on Silica Gel Catalyst Supports by n-Quantum Coherence in NMR. *Analytica Chimica Acta* **1993**, *283*, 1059–1079.

(39) Hwang, S.-J.; Uner, D. O.; King, T. S.; Pruski, M.; Gerstein, B. C. Characterization of Silica Catalyst Supports by Single and Multiple Quantum Proton NMR Spectroscopy. *J. Phys. Chem.* **1995**, *99*, 3697–3703.

(40) Chmelka, B. F.; Pearson, J. G.; Liu, S. B.; Ryoo, R.; Menorval, L. C. D.; Pines, A. NMR Study of the Distribution of Aromatic Molecules in NaY Zeolite. *J. Phys. Chem.* **1991**, *95*, 303–310.

(41) Hwang, S. J.; King, T. S.; Gerstein, B. C. Probing Intermediates in the Reaction of Ethylene Over Supported Ru; Use and Limitations of Multiple Quantum Spin Counting. *Catal. Lett.* **1991**, *8*, 367–373.

(42) Ryoo, R.; Liu, S. B.; Menorval, L. C. D.; Takegoshi, K.; Chmelka, B.; Trecoske, M.; Pines, A. Distribution of Hexamethylbenzene in a Zeolite Studied by Xenon-129 and Multiple-Quantum NMR. *J. Phys. Chem.* **1987**, *91*, 6575–6577.

(43) Hong, S. B.; Cho, H. M.; Davis, M. E. Distribution and Motion of Organic Guest Molecules in Zeolites. *J. Phys. Chem.* **1993**, *97*, 1622–1628.

(44) Hong, S. B.; Cho, H. M.; Davis, M. E. Location and Molecular Motion of Hexamethylbenzene in Zeolite NaY. *J. Phys. Chem.* **1993**, *97*, 1629–1633.

(45) Pearson, J. G.; Chmelka, B. F.; Shykind, D. N.; Pines, A. Multiple-quantum NMR study of the distribution of benzene in NaY zeolite. *J. Phys. Chem.* **1992**, *96*, 8517–8522.

(46) He, J.; Ba, Y.; Ratcliffe, C. I.; Ripmeester, J. A.; Klug, D. D.; Tse, J. S.; Preston, K. F. Encapsulation of Silicon Nanoclusters in Zeolite Y. *J. Am. Chem. Soc.* **1998**, *120*, 10697–10705.

(47) Geen, H.; Graf, R.; Heindrichs, A. S. D.; Hickman, B. S.; Schnell, I.; Spiess, H. W.; Titman, J. J. Spin Counting with Fast MAS. *J. Magn. Reson.* **1999**, *138*, 167–172.

(48) Saalwächter, K.; Spiess, H. W. Heteronuclear 1H–13C Multiple-Spin Correlation in Solid-State Nuclear Magnetic Resonance: Combining Rotational-Echo Double-Resonance Recoupling and Multiple-Quantum Spectroscopy. *J. Chem. Phys.* **2001**, *114*, 5707–5728.

(49) Baum, J.; Munowitz, M.; Garroway, A. N.; Pines, A. Multiplequantum Dynamics in Solid State NMR. *J. Chem. Phys.* **1985**, *83*, 2015–2025.

(50) Boettcher, S. W.; Bartl, M. H.; Hu, J. G.; Stucky, G. D. Structural Analysis of Hybrid Titania-Based Mesostructured Composites. *J. Am. Chem. Soc.* **2005**, *127*, 27.

(51) Baum, J.; Gleason, K. K.; Pines, A.; Garroway, A. N.; Reimer, J. A. Multiple-Quantum NMR Study of Clustering in Hydrogenated Amorphous Silicon. *Phys. Rev. Lett.* **1986**, *56*, 1377–1380.

(52) Saalwächter, K.; Ziegler, P.; Spyckerelle, O.; Haidar, B.; Vidal, A.; Sommer, J.-U. 1H Multiple-Quantum Nuclear Magnetic Resonance Investigations of Molecular Order Distributions in Polydimethylsiloxane Networks: Evidence for a Linear Mixing Law in Bimodal Systems. *J. Chem. Phys.* **2003**, *119*, 3468–3482.

(53) Gerasimowicz, W. V.; Garroway, A. N.; Miller, J. B.; Sander, L. C. Multiple-Quantum NMR Studies of Monomeric Bonded Silica Phases. *J. Phys. Chem.* **1992**, *96*, 9.

(54) Limb, S. J.; Scruggs, B. E.; Gleason, K. K. Distribution and Motion of Trifluoromethanesulfonate Anions in Poly(p-hydroxystyrene) and Polystyrene Films Studied by Multiple-Quantum NMR. *Macromolecules* **1993**, *26*, 3750–3757.

(55) Tycko, R. Selection Rules for Multiple Quantum NMR Excitation in Solids: Derivation from Time-Reversal Symmetry and Comparison with Simulations and 13C NMR Experiments. *J. Magn. Reson.* **1999**, *139*, 302–307.

(56) Balbach, J. J.; Ishii, Y.; Antzutkin, O. N.; Leapman, R. D.; Rizzo, N. W.; Dyda, F.; Reed, J.; Tycko, R. Amyloid Fibril Formation by A16-22, a Seven-Residue Fragment of the Alzheimer's -Amyloid Peptide, and Structural Characterization by Solid State NMR. *Biochem.* **2000**, *39*, 13748–13759.

(57) Tycko, R. Insights into the Amyloid Folding Problem from Solid-State NMR. *Biochem.* **2003**, *42*, 3151–3159.

(58) Oyler, N. A.; Tycko, R. Multiple Quantum 13C NMR Spectroscopy in Solids under High-Speed Magic-Angle Spinning. *J. Phys. Chem. B* **2002**, *106*, 8382–8389.

(59) Antzutkin, O. N.; Balbach, J. J.; Leapman, R. D.; Rizzo, N. W.; Reed, J.; Tycko, R. Multiple Quantum Solid-State NMR Indicates a Parallel, Not Antiparallel, Organization of -sheets in Alzheimer's -amyloid Fibrils. *PNAS* **2000**, *97*, 13045–13050.

(60) Dodd, A. J.; van Eck, E. R. H. Multiple Quantum Spin Counting Techniques with Quadrupolar Nuclei. *Solid State Nucl. Magn. Reson.* **2004**, *26*, 121–131.

(61) Tomaselli, M.; Meier, B. H.; Riccò, M.; Shiroka, T.; Sartori, A. A Multiple-Quantum Nuclear Magnetic Resonance Study of Interstitial Li Clusters in LixC60. *J. Chem. Phys.* **2001**, *115*, 472–476.

(62) Hughes, C. E. Spin Counting. *Prog. Nucl. Magn. Reson. Spectrosc.* **2004**, *45*, 301–313.

(63) Teymoori, G.; Pahari, B.; Stevensson, B.; Edén, M. Low-Power Broadband Homonuclear Dipolar Recoupling Without Decoupling: Double-Quantum 13C NMR Correlations at Very Fast Magic-Angle Spinning. *Chem. Phys. Lett.* **2012**, *547*, 103–109.

(64) Levitt, M. H. *Encyclopedia of Nuclear Magnetic Resonance: Advances in NMR*, 9th ed.; John Wiley & Sons: Chichester, UK, 2002.

(65) Teymoori, G.; Pahari, B.; Edén, M. Low-power broadband homonuclear dipolar recoupling in MAS NMR by two-fold symmetry pulse schemes for magnetization transfers and double-quantum excitation. *Journal of Magnetic Resonance* **2015**, *261*, 205–220.

(66) He, K.; Sawczyk, M.; Liu, C.; Yuan, Y.; Song, B.; Deivanayagam, R.; Nie, A.; Hu, X.; Dravid, V. P.; Lu, J.; Sukotjo, C.; peng Lu, Y.; Král, P.; Shokuhfar, T.; Shahbazian-

Yassar, R. Revealing Nanoscale Mineralization Pathways of Hydroxyapatite Using In Situ Liquid Cell Transmission Electron Microscopy. *Sci. Adv.* **2020**, *6*.

(67) Oyane, A.; Onuma, K.; Ito, A.; Kim, H.-M.; Kokubo, T.; Nakamura, T. Formation and Growth of Clusters in Conventional and New Kinds of Simulated Body Fluids. *J. Biomed. Mater. Res. A* **2002**, *64A*, 339–348.

(68) Oyane, A.; Kim, H.-M.; Furuya, T.; Kokubo, T.; Miyazaki, T.; Nakamura, T. Preparation and Assessment of Revised Simulated Body Fluids. *J. Biomed. Mater. Res. A* **2003**, *65A*, 188–195.

(69) Dey, A.; Bomans, P. H. H.; Müller, F. A.; Will, J.; Frederik, P. M.; de With, G.; Sommerdijk, N. A. J. M. The Role of Prenucleation Clusters in Surface-Induced Calcium Phosphate Crystallization. *Nat. Mater.* **2010**, *9*, 1010–1014.

(70) Equbal, A.; Jain, S. K.; Li, Y.; Tagami, K.; Wang, X.; Han, S. Role of Electron Spin Dynamics and Coupling Network in Designing Dynamic Nuclear Polarization. *Prog. Nucl. Magn. Reson. Spectrosc.* **2021**, *126-127*, 1–16.

(71) Li, Y.; Weng, W.; Cheng, K.; Du, P.; Shen, G.; Wang, J.; Han, G. Preparation of Amorphous Calcium Phosphate in the Presence of Poly(Ethylene Glycol). *J. Mater. Sci.* **2003**, *22*, 1015–1016.

(72) Ugurbil, K.; Holmsen, H.; Shulman, R. G. Adenine Nucleotide Storage and Secretion in Platelets as Studied by 31P Nuclear Magnetic Resonance. *PNAS* **1979**, *76*, 2227–2231.

(73) Zilm, M. E.; Chen, L.; Sharma, V.; McDannald, A.; Jain, M.; Ramprasada, R.; Wei, M. Hydroxyapatite Substituted by Transition Metals: Experiment and Theory. *Phys. Chem. Chem. Phys.* **2016**, *18*, 16457–16465.

(74) Freude, D.; Haase, J. *Quadrupole Effects in Solid-state NMR, Basic Principles and Experimental Techniques for Nuclei with Half-integer Spins*; quad-nmr.de, 2019.

(75) Brinkmann, A.; Edén, M. Central-Transition Double-Quantum Sideband NMR Spectroscopy of Half-Integer Quadrupolar Nuclei: Estimating Internuclear Distances and Probing Clusters within Multi-Spin Networks. *Phys. Chem. Chem. Phys.* **2014**, *16*, 7037–7050.

(76) Bretschneider, M.; Spindler, P. E.; Rogozhnikova, O. Y.; Trukhin, D. V.; Endeward, B.; Kuzhelev, A. A.; Bagryanskaya, E.; Tormyshev, V. M.; ; Prisner, T. F. Multiquantum Counting of Trityl Radicals. *J. Phys. Chem. Lett.* **2020**, *11*, 6268–6290.

(77) Oyler, N. A.; Tycko, R. Multiple Quantum 13C NMR Spectroscopy in Solids under High-Speed Magic-Angle Spinning. *J. Phys. Chem. B* **2002**, *106*, 8382–8389.

(78) Jain, S. K.; Tabassum, T.; Li, L.; Ren, L.; Fan, W.; Tsapatsis, M.; Caratzoulas, S.; Han, S.; Scott, S. L. P-Site Structural Diversity and Evolution in a Zeosil Catalyst. *J. Am. Chem. Soc.* **2021**, *143*, 1968–1983.

(79) Biedenbänder, T.; Aladin, V.; Saeidpour, S.; Corzilius, B. Dynamic Nuclear Polarization for Sensitivity Enhancement in Biomolecular Solid-State NMR. *Chem. Rev.* **2022**, *122*, 9738–9794.

(80) Tang, Y.; Zhou, Y.; Zhou, D.; Chen, Y.; Xiao, Z.; Shi, J.; Liu, J.; Hong, W. Electric Field-Induced Assembly in Single-Stacking Terphenyl Junctions. *J. Am. Chem. Soc.* **2020**, *142*, 19101–19109.

(81) Fisher, M. P. Quantum Cognition: The Possibility of Processing with Nuclear Spins in the Brain. *Ann. Phys.* **2015**, *362*, 593–602.

(82) Posner, A. S.; Betts, F. Synthetic Amorphous Calcium Phosphate and Its Relation to Bone Mineral Structure. *Bone Mineral Structure* **1975**, *8*, 273–281.

(83) Posner, A. S.; Betts, F.; Blumenthal, N. C. Formation and Structure of Synthetic and Bone Hydroxyapatites. *Prog. Cryst. Growth Charact. Mater.* **1980**, *3*, 49–64.

(84) Campana, V.; Milano, G.; Pagano, E.; Barba, M.; Cicione, C.; Salonna, G.; Lattanzi, W.; Logroscino, G. Bone Substitutes in Orthopaedic Surgery: From Basic Science to Clinical Practice. *J. Mater. Sci. Mater. Med.* **2014**, *25*, 2445–61.